MNRAS **000**, 000–000 (0000) Preprint 19 July 2016 Compiled using MNRAS LATEX style file v3.0

Imprint of thawing scalar fields on large scale galaxy overdensity

Bikash R. Dinda ⋆, Anjan A Sen †
Centre for Theoretical Physics, Jamia Millia Islamia, New Delhi-110025, India.

19 July 2016

arXiv:1607.05123v1 [astro-ph.CO] 18 Jul 2016

ABSTRACT

We calculate the observed galaxy power spectrum for the thawing class of scalar field models taking into account various general relativistic corrections that occur on very large scales. As we need to consider the fluctuations in scalar field on these large scales, the general relativistic corrections in thawing scalar field models are distinctly different from ΛCDM and the difference can be upto $15-20\%$ at some scales. Also there is an interpolation between suppression and enhancement of power in scalar field models compared to the ΛCDM model on smaller scales and this happens in a specific redshift range that is quite robust to the form of the scalar field potentials or the choice of different cosmological parameters. This can be useful to distinguish scalar field models from ΛCDM with future optical/radio surveys.

Key words: cosmology: theory – large-scale structure of Universe - cosmology: Dark energy

1 INTRODUCTION

Since the first observational evidence for the late time acceleration of the universe (Perlmutter et al. 1997; Riess et al. 1998), it has been the biggest challenge in theoretical as well as obsevational cosmology to find the source of the repulsive gravitational force that causes this acceleration. We still do not have confirmatory evidence whether this is due to some extra dark component in the energy budget of the universe (commonly called as "dark energy") (Sahni & Starobinsky 2000; Peebles & Ratra 2003; Padmanabhan 2003) or due to some modification of Einstein gravity on cosmological scales (Tsujikawa 2010). Although the Planck-2015 result (Ade et al. 2015a) shows that the concordance ΛCDM universe is consistent with a whole set of observational data, still there are some recent observational results that indicate inconsistency with ΛCDM model (Sahni et al. 2014; Delubac et al. 2015; Riess et al. 2016; Bonvin et al. 2016). This is in addition to the theoretical inconsistencies like fine tuning and cosmic coincidence problems that are present in ΛCDM model. This motivates people to go beyond ΛCDM model and to consider models with evolving dark energy.

But one needs to distinguish this evolving dark energy from a cosmological constant (Λ) which does not change through out the history of the universe. To do so, we need to study the effect of both on different cosmological observables related to background expanding universe as well as to the process of growth of structures in our universe. This can be done through observations with Supernova Type-Ia as standard candles (Betoule et al. 2014), or observing the fluctuations in the temperature of cosmic microwave background radiation (CMBR) (Ade et al. 2015a) or looking at the galaxies and their distribution over different distance scales as well as at different redshifts (Alam et al. 2016). The latest Planck results in 2015 together with data from Supernova Type-Ia and also data related to Baryon Acoustic Oscillations (BAO) from different redshift surveys have put unprecedented constraints on different cosmological parameters including those related to dark energy properties (Ade et al. 2015a,b). But as far as the dark energy is concerned, we have mainly constrained its background evolution till now. This is because most of the observations mentioned above are either related to background universe, or perturbed universe on sub-horizon scales where Newtonian treatment is sufficient and one can safely ignore the fluctuations in dark energy. Hence it has not been possible till now to probe the inhomogeneity in dark energy which can be very useful in distinguishing different dark energy models.

Future optical as well as radio/infrared surveys like LSST (Abell et al. 2009), SKA (Maartens et al. 2015) etc, have potential to cover larger sky area and to extend to much higher redshifts probing horizon scales and beyond. This will give us a whole lot of information about our universe on such large length scales which is not known yet. Crucially on these scales, one needs to consider the full general relativistic (GR) treatment to study how fluctuations grow and dark energy perturbation can not be neglected any more. This can be a smoking gun to distinguish evolving dark energy model from ΛCDM as Λ, being a constant is not perturbed whereas any other evolving dark energy component should be perturbed and hence has different GR correction from Λ.

⋆ E-mail:bikash@ctp-jamia.res.in
† aasen@jmi.ac.in

© 0000 The Authors

In general there are two broad categories of GR corrections to the simple Newtonian treatment that is usually considered for sub-horizon scales. One is related to the evolving gravitational potential which can be local or at the observed galaxies or along the line of sight and the other is related to the peculiar velocities due to the motion of galaxies relative to the local observer. In recent years, there has been number of studies related to the calculation of power spectrum of galaxy overdensity using full general relativistic treament (Yoo et al. 2009; Bonvin & Durrer 2011; Challinor & Lewis 2011; Jeong et al. 2012; Yoo et al. 2012; Bertacca et al. 2012; Duniya 2016). This has been done mostly in the context of ΛCDM universe.

The simple way to consider evolving dark energy model is a canonical scalar field rolling over its potential. The first such model considered was the "tracker" scalar field model (Wetterich 1988; Copeland et al. 2006; Ratra & Peebles 1988; Caldwell et al. 1998; Liddle & Scherrer 1999; Steinhardt et al. 1999) with some particular types of potential that causes the scalar field to track the background radiation/matter component until recent past when slope of the potential changes so that it can behave as Λ and causes the universe to accelerate. This tracker behaviour helps to evade the cosmic coincidence problem that is present in the ΛCDM model. GR effect on horizon scales for tracker scalar field model has been studied recently by Duniya et al (Duniya et al. 2013).

It has been recently argued that constraints on dark energy equation of state as well as its contribution to the energy budget of the universe during recombination disfavour the tracker scalar field models (Linder 2015). Also the recent analysis of spectrum from a distant quasar indicates that the dark energy scalar field has not evolved appreciably during much of the history of the universe (Bagdonaite et al. 2015). This also disfavours tracker scalar field model where the scalar field fast rolls for a very long time during its early stages of evolution.

This motivates people to consider another kind of scalar field models, “the thawer class”, (Caldwell & Linder 2005) where the scalar field is initially frozen at some flat part of the potential due to large Hubble friction in the early time and behaves like a cosmological constant with $w \approx -1$. Later on, as the Hubble friction decreases, the scalar field slowly thaws away from its initial frozen state and evolves away from cosmological constant type behaviour. In this case, the scalar field never evolves much from its initial frozen state and the equation of state always remain very close to $w = -1$. Thawer scalar fields are much similar to the inflaton that drives the acceleration in the universe in the early time. It is also interesting to note that the thawer canonical scalar field model has a generic analytical behaviour for its equation of state for nearly flat potentials (Scherrer & Sen 2008) (Also see (Li & Scherrer 2016) for the generalisation of this result for non-canonical scalar field). Thawing model in the context of tachyon field (Ali et al. 2009) as well as galileon field (Hossain & Sen 2012) have been also considered in the recent past.

In this paper we study the full general relativistic treatment for the growth of linear fluctuations in cosmological models with thawing scalar field as dark energy. We study the power spectrum of galaxy overdensity taking into account various GR corrections and compare that with ΛCDM model. We also study the possibility to distinguish individual potentials for the scalar field at horizon and superhorizn scales.

The paper is organized as follows: in section 2, we briefly describe the background equations for the thawing dark energy models; in section 3, we describe the full general relativistic perturbation equation for linear fluctuations in both dark energy and matter, form a single set of autonomous equations involving both background evolution and evolution for the fluctuations and study various cosmological quatities; in section 4, we calculate the observed galaxy power spectrum taking into account various GR correction terms for different scalar field potentials and compare them with ΛCDM model; in section 5, we mention our conclusions.

2 BACKGROUND EVOLUTION

We consider flat FLRW background geometry for our Universe with $a(t)$ being the scale factor. The Lagrangian density for a minimally coupled canonical scalar field ϕ is given by

$$\mathcal{L} = \frac{1}{2}(\partial^\mu\phi)(\partial_\mu\phi) - V(\phi). \tag{1}$$

Here $V(\phi)$ is the potential for the field ϕ. The background energy density and pressure of the scalar field are given by

$$\begin{aligned}\bar{\rho_\phi} &= \frac{1}{2}\dot{\phi}^2 + V(\phi),\\ \bar{P_\phi} &= \frac{1}{2}\dot{\phi}^2 - V(\phi),\end{aligned} \tag{2}$$

where overdot represents derivative with respect to the cosmic time t. The equation of motion for the scalar field is given by

$$\ddot{\phi} + 3H\dot{\phi} + V_\phi = 0, \tag{3}$$

where H is the Hubble parameter and subscript ϕ is the derivative w.r.t the field ϕ. The background Friedmann equation is given by

$$3M_{pl}^2H^2 = \bar{\rho}_m + \bar{\rho}_\phi, \tag{4}$$

where $M_{pl} = (8\pi G)^{-1/2}$, G being the Newton’s gravitational constant, is the Planck’s mass. $\bar{\rho}_m$ is the energy density of the background matter component which includes contribution from dark matter and baryons.

3 RELATIVISTIC PERTURBATIONS WITH SCALAR FIELD

We assume conformal Newtonian gauge with vanishing anisotropic stress for the perturbed space-time:

$$ds^2 = a^2(\tau)[(1+2\Phi)d\tau^2 - (1-2\Phi)d\vec{x}.d\vec{x}], \tag{5}$$

where τ is the conformal time, Φ is the gravitational potential and $\vec{x}$ are the comoving coordinates. The linearised Einstein equations are now given by (Unnikrishnan et al. 2008):

$$\nabla^2\Phi - 3\mathcal{H}(\Phi' + \mathcal{H}\Phi) = 4\pi G a^2 \sum_i \delta\rho_i, \tag{6}$$

$$\Phi' + \mathcal{H}\Phi = 4\pi G a^2 \sum_i (\bar{\rho}_i + \bar{P}_i)v_i, \tag{7}$$

$$\Phi'' + 3\mathcal{H}\Phi' + (2\mathcal{H}' + \mathcal{H}^2)\Phi = 4\pi G a^2 \sum_i \delta P_i, \tag{8}$$

where prime is the derivative with respect to the conformal time τ, $\mathcal{H}$ is the conformal Hubble parameter, $\bar{\rho}_i$ and $\bar{P}_i$ are the background energy density and pressure for the individual fluid i (here i stands for either 'm' for matter or 'ϕ' for scalar field) and $\delta\rho_i$, δP_i and v_i are the perturbation to individual component's background energy density, pressure and velocity field respectively. The irrotational part of individual velocity field is given by $\vec{v_i} = -\vec{\nabla}v_i$. Combining eqs. (6) and (7) we can get the relativistic Poisson equation as

$$\nabla^2\Phi = 4\pi G a^2 \sum_i \bar{\rho}_i \Delta_i, \tag{9}$$

where $\Delta_i = \delta_i + 3\mathcal{H}(1+w_i)v_i$ is the comoving energy density contrast for individual component and they are the correct tracer of the gravitational potential on large scales.
From the conservation of stress-energy tensor we can get relativistic continuity and Euler equations as

$$\delta' + 3\mathcal{H}(\frac{\delta P}{\delta\rho} - \frac{\bar{P}}{\bar{\rho}})\delta = (1+\frac{\bar{P}}{\bar{\rho}})(\theta + 3\Phi') \tag{10}$$

and

$$\theta' + 3\mathcal{H}(\frac{1}{3} - \frac{\bar{P}'}{\bar{\rho}'})\theta = \frac{\nabla^2\delta P}{\bar{\rho}+\bar{P}} + \nabla^2\Phi \tag{11}$$

respectively where $\theta = \vec{\nabla}.\vec{v}$ and δ is defined as $\delta\rho = \bar{\rho}\delta$. Note that the above continuity and Euler equations are valid for individual components e.g. matter or scalar field and also for the combined (matter plus dark energy) one.

For scalar field ϕ, the perturbed energy density, pressure and velocity (at linear order) are given by

$$\delta\rho_\phi = \frac{\phi'(\delta\phi')}{a^2} - \frac{\phi'^2\Phi}{a^2} + V_\phi\delta\phi, \tag{12}$$

$$\delta P_\phi = \frac{\phi'(\delta\phi')}{a^2} - \frac{\phi'^2\Phi}{a^2} - V_\phi\delta\phi, \tag{13}$$

and

$$a(\bar{\rho_\phi} + \bar{P}_\phi)v_\phi = \frac{\phi'}{a}(\delta\phi), \tag{14}$$

where $\delta\phi$ is the perturbation to the background field ϕ.

We now define the following dimensionless quantities related to the background (Scherrer & Sen 2008) as well as perturbed universe:

$$
\begin{aligned}
x &= \frac{\left(\frac{d\phi}{dN}\right)}{\sqrt{6}M_{Pl}}, \qquad & y &= \frac{\sqrt{V}}{\sqrt{3}HM_{Pl}}, \\
\lambda &= -M_{Pl}\frac{V_\phi}{V}, \qquad & \Gamma &= V\frac{V_{\phi\phi}}{V_\phi^2}, \\
\Omega_\phi &= x^2+y^2, \qquad & \gamma &= 1+w = \frac{2x^2}{x^2+y^2}, \\
q &= (\delta\phi)/\frac{d\phi}{dN}. & & \qquad (15)
\end{aligned}
$$

where $N = log(a)$ is the number of e-folding. The x here is different from the comoving coordinates in equation (5). Here Ω_ϕ is the density parameter related to the scalar field, w is the equation of state for the scalar field. With these quantities, one can now form a single set of autonomous system of equations involving quantities related to both the background (Scherrer & Sen 2008) as well as perturbed universe as following:

$$
\begin{aligned}
\frac{d\gamma}{dN} &= 3\gamma(\gamma-2)+\sqrt{3\gamma\Omega_\phi}(2-\gamma)\lambda, \\
\frac{d\Omega_\phi}{dN} &= 3(1-\gamma)\Omega_\phi(1-\Omega_\phi), \\
\frac{d\lambda}{dN} &= \sqrt{3\gamma\Omega_\phi}\lambda^2(1-\Gamma), \\
\frac{d\mathcal{H}}{dN} &= -\frac{1}{2}(1+3(\gamma-1)\Omega_\phi)\mathcal{H} \\
\frac{d\Phi}{dN} &= \Phi_1 \\
\frac{dq}{dN} &= q_1 \\
\frac{d\Phi_1}{dN} &= -(1+B)\Phi_1-(2B-3+1.5\gamma\Omega_\phi)\Phi+1.5\gamma\Omega_\phi\Big[q_1+(2g-B)q\Big] \\
\frac{dq_1}{dN} &= -(2g-B)q_1-B_q q+4\Phi_1+2g\Phi. \qquad (16)
\end{aligned}
$$

Here $B = 1.5(1-(\gamma-1)\Omega_\phi)$, $B_q = 6g - \frac{dB}{dN} - 2Bg + \frac{k^2}{\mathcal{H}^2}$ and $g = \sqrt{1.5}\lambda y^2/x$ where x and y can be easily written in terms of γ and Ω_ϕ using equation (15).

Note that in the above set of equations, equations involving Φ and q are written in Fourier space where for simplicity we have taken the same notations in the Fourier space for corresponding entities. Using Fourier version of eqs. (6) and (12) and changing the τ derivative to the derivative w.r.t N, we get matter density contrast as given by

$$
\delta_m = -\frac{2}{\Omega_m}\Big[\frac{d\Phi}{dN}+\Big(1-x^2+\frac{k^2}{3\mathcal{H}^2}\Big)\Phi+x^2\Big(\frac{dq}{dN}-Bq\Big)\Big]. \qquad (17)
$$

Similarly, using Fourier version of eqs. (7) and (14), we get peculiar velocity for matter as

$$
y_m = 3\mathcal{H}v_m = \frac{2}{\Omega_m}\Big[\frac{d\Phi}{dN}+\Phi-3x^2q\Big]. \qquad (18)
$$

Using eqs. (17) and (18), we get co-moving matter density contrast as $\Delta_m = \delta_m + y_m$.

3.1 Initial conditions

To solve the system of equation (16), we need initial conditions for $(\gamma, \Omega_\phi, \lambda, \mathcal{H})$ for the background universe and $(\Phi, \frac{d\Phi}{dN}, q, \frac{dq}{dN})$ for the perturbed universe. We set our initial condition at decoupling ($z = 1000$), which ensures that there is negligible dark energy contribution at that time and the universe is matter dominated.

As we are considering the thawing class of models where the scalar field is initially frozen due to large Hubble friction at $w \sim -1$, $\gamma_i \sim 0$ initially. We set it at 10^{-7}. Our results are not very sensitive to this value as long $\gamma_i << 1$. The initial value for Ω_ϕ is also negligible (at $z = 1000$, we do not expect any contribution from dark energy). Initial value for λ, the slope of the potential, is an important quantity. It determines the subsequent evolution of the scalar field. For $\lambda_{in} << 1$, the scalar field does not evolve much from its initial frozen state and always stays very close to the cosmological constant behaviour. For large values of λ_i, the scalar field can thaws away substantially from its initial frozen state $w \sim -1$. In our case, we fix the initial values for Ω_ϕ, λ and $\mathcal{H}$ to set Ω_ϕ and w at present ($z = 0$) to their desired values and to ensure that $\frac{\mathcal{H}}{\mathcal{H}_0}$ is equal to 1 at present ($z = 0$).

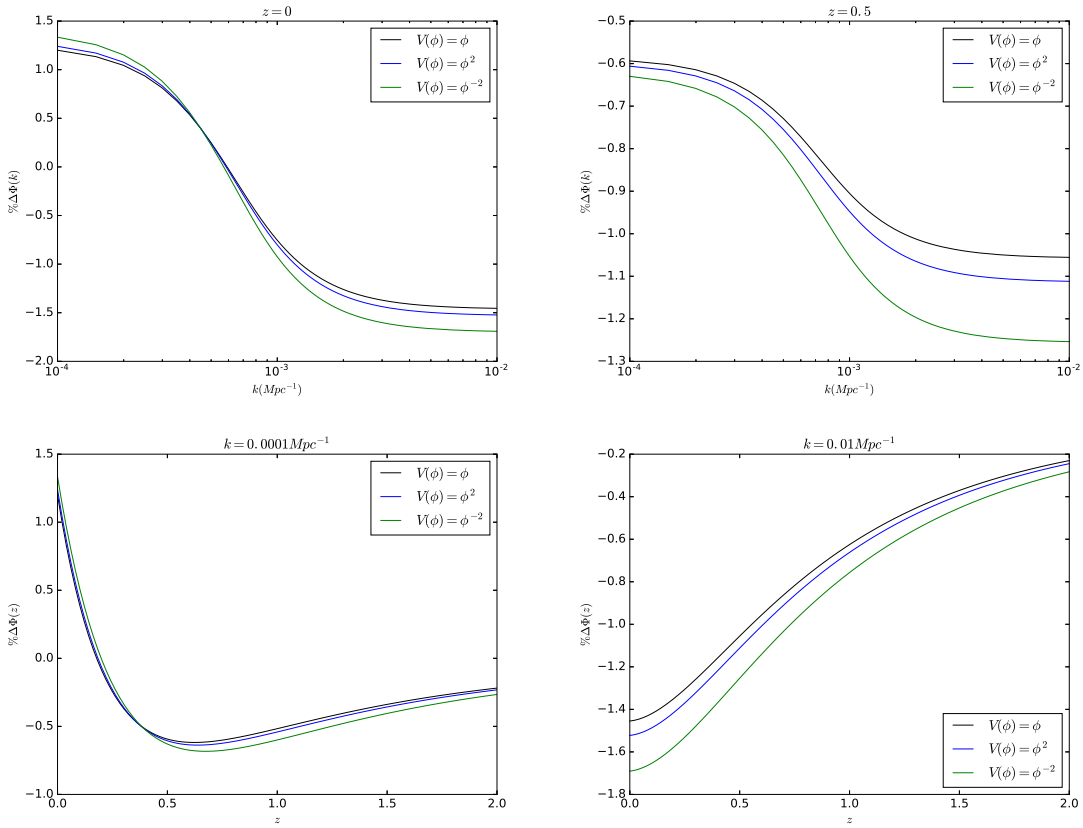

Figure 1. Percentage deviation in Φ from ΛCDM model: negative values in y-axis means they are all suppressed from ΛCDM. $\Omega_{m0} = 0.28$ and $w_0 = -0.9$ in these plots.

For the scalar field perturbation, we assume it is negligible initially as there is hardly any contribution from dark energy at $z = 1000$ and we set $q = \dfrac{dq}{dN} = 0$ initially.

To set the initial condition for the gravitational potential Φ, we know that, during matter domination, Φ is constant and hence $\dfrac{d\Phi}{dN} = 0$ initially. Also during matter domination, $\Delta_m \sim a$ and using the Poisson equation, one can easily show

$$\Phi_{in} = -\frac{3}{2}\frac{\mathcal{H}_{in}^2}{k^2} a_{in}. \tag{19}$$

3.2 Behaviour of different cosmological parameters

With the system of autonomous equations given in (16) and the initial conditions described above, we solve the set of equations and study various cosmological parameters. For this purpose we concentrate on power-law potentials, more specifically the linear, squared and inverse-squared potentials. It is straightforward to generalise our study for more exotic potentials. We also fix the following quantities for our purpose: $\Omega_{m0} = 0.28$ and $w_0 = -0.9$. We shall discuss later what happens if one deviates from these values. This, together with the condition that $\frac{\mathcal{H}}{\mathcal{H}_0} = 1$ at $z = 0$, fixes $\Omega_{\phi i}$, λ_i and $\mathcal{H}_i$.

To start with, we plot in figure 1 the behaviour of the gravitational potential Φ. We show the deviation from ΛCDM model for each scalar field potential. We show this deviation as a function of scale 'k' for two different redshifts and also as a function of redshift 'z' for different scales. As one can see, the deviation asymptotes to approximately $1 - 2\%$ for both higher and smaller k. For higher k (smaller scales) the deviation is slightly higher than that from $k = 0.0001 Mpc^{-1}$. The deviation decreases with redshifts. Also interestingly for larger scales, the gravitational potential Φ is enhanced in scalar field models than the ΛCDM model, where as for smaller scales it is suppressed. This happens at redshift $z = 0$; for larger redshift, there is always a suppression with respect to ΛCDM. Also the inverse-squared potential has a larger deviation from ΛCDM model compared to linear and squared potentials.

In figure 2, we show the behaviour of comoving matter density contrast Δ_m. Here also we plot the deviation from ΛCDM model for

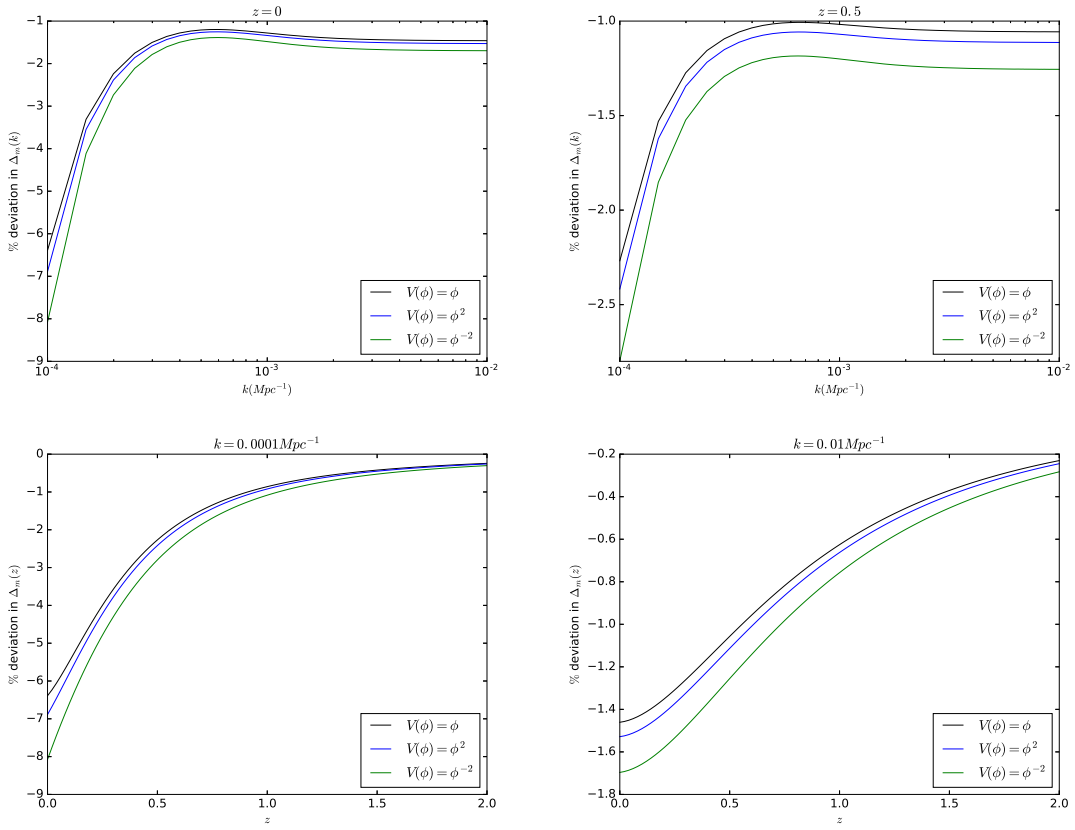

Figure 2. Percentage deviation in Δ_m from ΛCDM model: negative values in y-axis means they are all suppressed from ΛCDM. $\Omega_{m0} = 0.28$ and $w_0 = -0.9$ in these plots.

each of the potentials. Again inverse-squared potential has the largest deviation from ΛCDM compared to the linear and squared potential. On larger scales, the deviations are much larger than what we observe in the gravitational potential. One can get upto $7 - 8\%$ deviations at $z = 0$ and upto 3% deviation at $z = 0.5$ for $k = 0.0001 Mpc^{-1}$. On smaller scales, the deviations are smaller and similar to that in gravitational potential Φ. This is because on smaller scales the contribution from dark energy perturbation is negligible and Δ_m exactly traces the gravitational potential Φ. Also in this case, there is always suppressions from ΛCDM model unlike gravitational potential where there is a enhancement from ΛCDM on larger scales. This reason is on larger scales the dark energy perturbation also contributes to the total gravitational potential Φ which is otherwise absent in ΛCDM case due to constant Λ.

Next we study the parameter $f = -\frac{k^2 v_m}{\mathcal{H}\Delta_m}$ that determines the redshift space distortion (Duniya 2016). For concordance model, it is identical to the standard growth function $f_s = \frac{d\log\Delta_m}{d\log a}$. In figure 3, we plot the deviation in f from ΛCDM model for each of the potentials. Here also inverse-squared potential has the largest deviation as we observe in Φ and Δ_m behaviour. At $z = 0$, there is enhancement upto $6 - 7\%$ at $k = 0.0001 Mpc^{-1}$ from ΛCDM for different potentials whereas for higher redshifts, there is always a suppression from ΛCDM. This suppression is highest around $z = 0.5$ (around $2 - 2.5\%$) and then decreases subsequently independent of the scale. Given the fact that this quantity controls the redshift space distortion term (Kaiser effect) in the observed galaxy power spectrum, it is interesting to see how it affects the observed power spectrum at different scales and different redshifts. We shall discuss this in the next section.

4 THE OBSERVED GALAXY POWER SPECTRUM

Distribution of galaxies in our universe is one of the best possible probes to study the evolution of our universe and its contents. Observed galaxy distribution is related to the underlying dark matter distribution and hence by observing various features in the galaxy distribution at different scales, one can study the growth in dark matter fluctuations which in turn can help us to distinguish various dark energy and modified gravity models.

In late eighties, Kaiser (Kaiser 1987) argued that we do not see galaxies in real space but in redshift space and its distribution in redshift

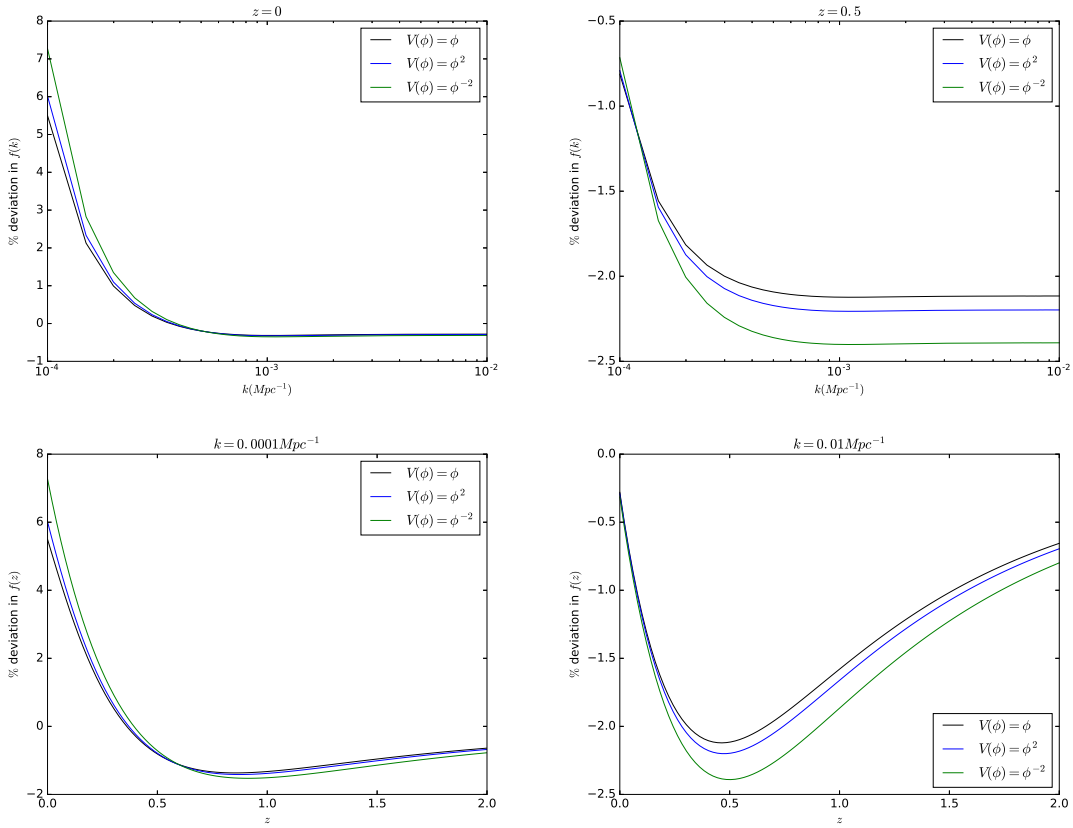

Figure 3. Percentage deviation in f from ΛCDM model: negative values in y-axis means they are all suppressed from ΛCDM. $\Omega_{m0} = 0.28$ and $w_0 = -0.9$ in these plots.

space is influenced also by the peculiar velocities of the galaxies in addition to the dark matter fluctuations. This gives rise to what is known as the Kaiser redshift space distortion, a measure of the large scale velocity field. This contains valuable information about the underlying cosmology.

In addition, the observed galaxy distribution is also affected by gravitational lensing through an effect known as magnification bias (Moessner et al. 1998), allowing the faint galaxies to be detected through the magnification due to lensing effect. This depends on the gravitational potentials in the metric integrated along the photon geodesics.

In recent years, people have shown the presence of other effects in the observed galaxy distribution on larger scales. These are purely general relativistic effects and depends on how the gravitational potential, velocity fields as well as the matter density affect the observed number density of galaxies on large cosmological scales (Yoo et al. 2009; Bonvin & Durrer 2011; Challinor & Lewis 2011; Jeong et al. 2012). On sub horizon scales, these GR effects are negligible in comparison to other effects like redshift space distortion. However on large cosmological scales, where one needs to consider full general relativistic treatment, they can be important in distinguishing different dark energy models.

In a galaxy survey, we observe the fluctuations in the number of galaxies across the sky and at different redshifts and angles. The galaxy number overdensity defined as $\Delta^{obs} = \frac{N(z,\vec{n}) - \bar{N}(z)}{N(z)}$ (Bonvin 2014), where $\vec{n}$ denotes the direction of observation, $N(z, \vec{n})$ denotes the observed number of galaxies detected at redshift bin of size δz centred at z and along direction $\vec{n}$ and $\bar{N}(z)$ is the mean number of galaxies at z, is given by (Duniya 2016; Duniya et al. 2013, 2015; Challinor & Lewis 2011)

$$\Delta^{obs} = \left[b + f\mu^2 + \mathcal{A}(\frac{\mathcal{H}}{k})^2 + i\mu\mathcal{B}(\frac{\mathcal{H}}{k}) \right] \Delta_m, \tag{20}$$

where b is the scale independent bias on linear scales that relates the dark matter density contrast to the galaxy density contrast, f the redshift space distortion parameter that is defined in the previous section, $\mu = -\frac{\vec{n}.\vec{k}}{k}$ with $\vec{k}$ being the wave vector and k being the wavenumber. $\mathcal{A}$ and $\mathcal{B}$ are defined as:

$$\mathcal{A} = 3f + (\frac{k}{\mathcal{H}})^2 \Big[3 + \frac{\mathcal{H}'}{\mathcal{H}^2} + \frac{\Phi'}{\mathcal{H}\Phi} \Big] \frac{\Phi}{\Delta_m}, \tag{21}$$

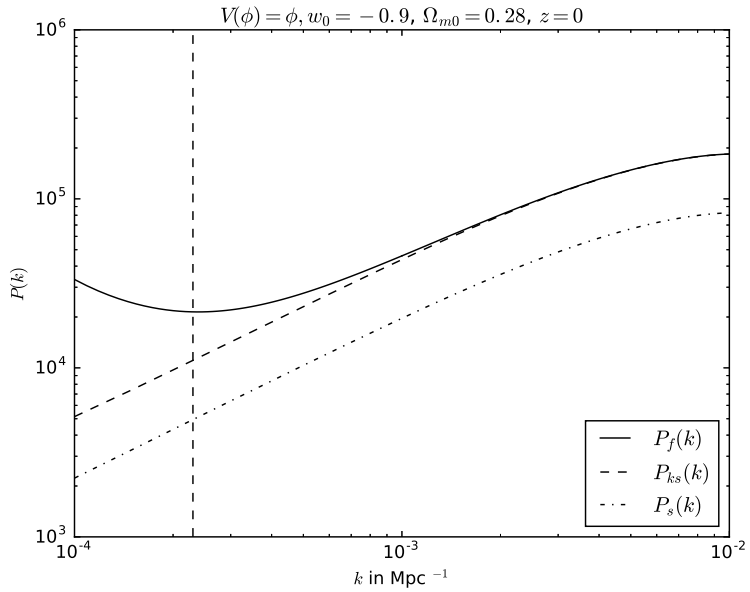

Figure 4. Dashed-dotted, dashed and continuous lines are for the usual matter power spectrum P_s (given by eqn (24)), the galaxy power spectrum taking only Kaiser term P_{ks} (Taking only the first term inside square bracket in eqn (23)) and the full observed galaxy power spectrum P_f given by eqn. (23) respectively. The vertical line is the horizon scales at $z = 0$.

$$\mathcal{B} = -\Big[2 + \frac{\mathcal{H}'}{\mathcal{H}^2}\Big] f. \tag{22}$$

Here we assume the magnification bias $\mathcal{Q}$ to be equal unity (Duniya et al. 2015) and also assume a constant comoving galaxy number density for which the galaxy evolution bias $b_e = 0$. We also neglect the time-delay, ISW and weak lensing integrated terms. The first term inside square bracket in equation (20) is related to galaxy bias, the second term is the Kaiser redshift space distortion term. The parameters $\mathcal{A}$ and $\mathcal{B}$ are related to the GR correction. $\mathcal{A}$ is related to the peculiar velocity potential and the gravitation potential whereas $\mathcal{B}$ is related to the Doppler effect. Using (20), one can now write the power spectrum for the observed galaxy overdensity (the real part) as (Duniya 2016; Duniya et al. 2013, 2015; Challinor & Lewis 2011):

$$P_f(k,z) = \left[(b + f\mu^2)^2 + 2(b + f\mu^2)\Big(\frac{\mathcal{A}}{y^2}\Big) + \frac{\mathcal{A}^2}{y^4} + \mu^2\Big(\frac{\mathcal{B}^2}{y^2}\Big)\right] P_s(k,z), \tag{23}$$

where $y = \frac{k}{\mathcal{H}}$ and P_s is the standard matter power spectra given by

$$P_s(k,z) = Ak^{n_s} T(k)^2 \left(\frac{\Delta_m(k,z)}{\Delta_m(k,0)}\right)^2. \tag{24}$$

In the above equation for P_s, we fix the constant A using σ_8 normalization and we use the Eisenstein-Hu transfer function for $T(k)$. In figure 4, we plot the line of sight ($\mu = 1$) observed galaxy power spectrum given by equation (23) for the linear potential only. We assume the spectral index for the initial power spectrum $n_s = 0.96$, $\sigma_8 = 0.8$, $h = 0.7$ and $\Omega_{b0} = 0.05$ for our calculation. The behaviour of the total power spectrum clearly shows the enhancement of power on larger scales due to GR corrections as compared to the standard matter power spectrum or when one includes only the Kaiser redshift space distortion term.

Next we show the deviation in observed galaxy power spectrum from the ΛCDM value for different scalar field potentials. We show it for the standard power spectrum P_s, power spectrum with Kaiser term only P_{ks} and for the full power spectrum P_f with GR corrections. We show the deviation as function of redshift for two different scales $k = 0.0001 Mpc^{-1}$ and $k = 0.0005 Mpc^{-1}$. For larger k, the deviation is much smaller. The result is shown in figure 5. For the full observed galaxy power spectrum one can get upto $15-20\%$ enhancement from the ΛCDM model for $k = 0.0001 Mpc^{-1}$ and for different redshifts. Inverse-squared potential has the largest deviation freom ΛCDM. Within individual potentials, there is a 5% deviation between linear and inverse-squared potential. For smaller scales ($k \sim 0.0005 Mpc^{-1}$), the deviation reduces substantially but interestingly we now have suppression of power from ΛCDM model for smaller redshifts and enhancement of power from ΛCDM for higher redshifts irrespective of the potential. This suppression is also present for certain potentials at $k = 0.0001 Mpc^{-1}$

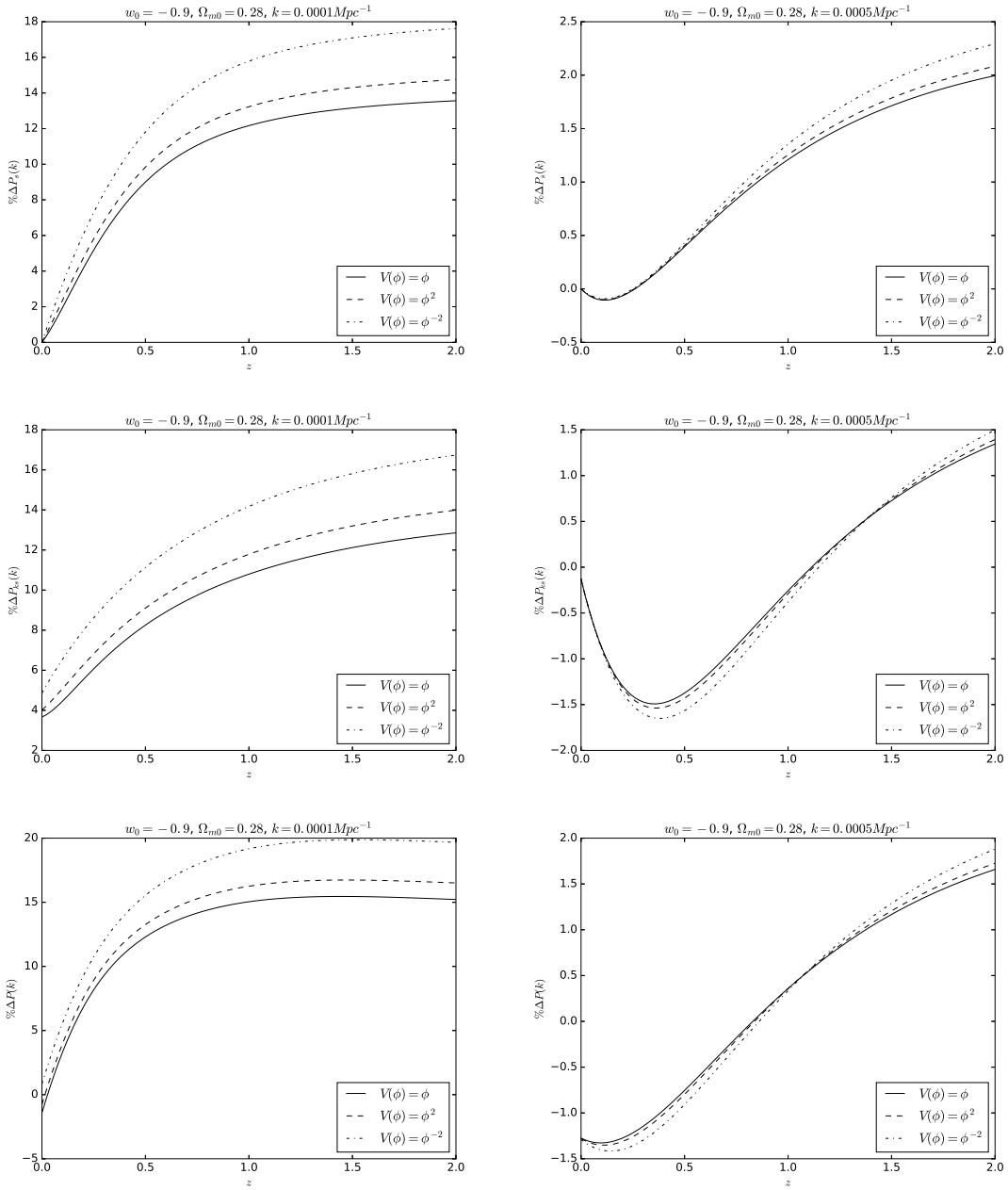

Figure 5. Percentage deviation in $P(k)$ from ΛCDM model for different potentials: negative values in y-axis means they are all suppressed from ΛCDM. Top most plots are standard matter power spectra P_s given by eqn. (24), middle plots are for power spectra with Kaiser redshift space distortion term included and the bottom ones for full observed galaxy power spectra P_f given by eqn (23) with GR corrections.

but around $z \sim 0$. But at $k = 0.0005 Mpc^{-1}$, this suppression shifts to redshift around $z \sim 1.2$ and this is primarily driven by the Kaiser term as shown in the plot for P_{ks}. For higher redshifts, there is again an enhancement in power with respect to ΛCDM.

To see how it behaves for smaller scales, in figure 6, we plot the same for $k = 0.001 Mpc^{-1}$ and for $k = 0.05 Mpc^{-1}$ and the result is similar to what we show for $k = 0.0005 Mpc^{-1}$. This change in slope in the galaxy power spectrum with respect to the ΛCDM model is an interesting signature for thawing scalar field models that we consider in our analysis and can be useful to test dark energy models with future data. Even if the deviation on smaller scales are much smaller than that at $k = 0.0001 Mpc^{-1}$ but this interpolation between enhancement and suppression of power with respect to ΛCDM is a distinguishable feature for thawing dark energy model and may be for any evolving dark energy models. Also in these plots, the change over from suppression to enhancement of power at smaller scales occurs around redshift around $z \sim 1.2$.

To study the dependence of this redshift to other cosmological parameters, we redo the analysis for a different combination $\Omega_{m0} = 0.25$ and $w_0 = -0.95$. The result is shown in figure 7. As one can see, although the deviation from ΛCDM is smaller than the previous combination

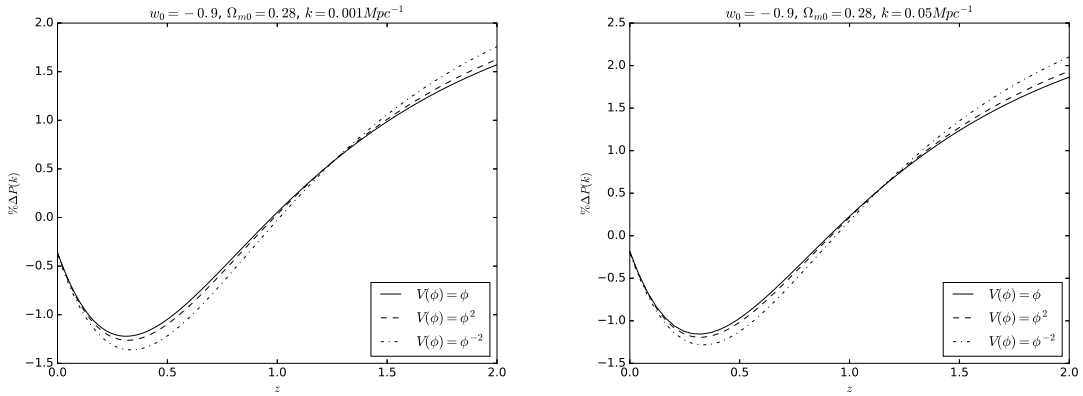

Figure 6. Percentage deviation in $P_f(k)$ from ΛCDM model for different potentials: negative values in y-axis means they are all suppressed from ΛCDM.

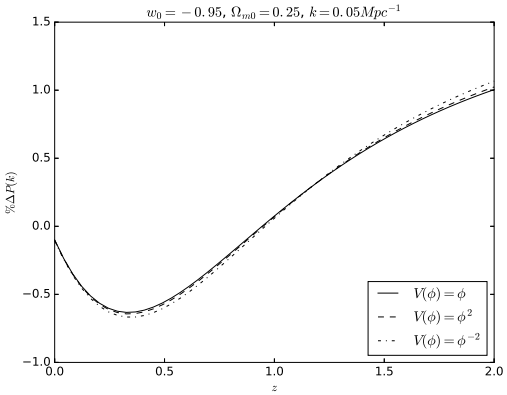

Figure 7. Same as figure 6 but with $\Omega_{m0} = 0.25$ and $w_0 = -0.95$.

of $\Omega_{\rm m0}$ and w_0, but the change over from enhancement to suppression of power with respect to ΛCDM happens again around $z \sim 1.2$. Hence this changeover redshift is quite robust in terms of different potentials and different cosmological parameters which is very interesting observationally. Because if we observe observe the power spectra around this redshift, we expect to see features that may help us to distinguish between ΛCDM and a evolving dark energy like thawing scalar field.

5 CONCLUSION

Future survey like LSST, SKA etc have the potential to probe our universe on very large scales and also at very higher redshifts. This will give us the opportunity to probe the general relativistic effects on large scale structure formations. As we start probing universe on very large scales, we can not ignore the dark energy perturbations and hence all the GR corrections in observed galaxy power spectrum contain the contribution from dark energy perturbations. This is indeed very promising as we can now distinguish ΛCDM model (where there is no dark energy perturbation) from other evolving dark energy models (where dark energy perturbations are present) in a completely new way which has not been possible till now. Hence it is important to study the observed galaxy power spectra with relevant GR corrections for different non-ΛCDM dark energy models.

In this work we do this for thawing scalar field models for dark energy which is a natural alternative to ΛCDM model. These are similar models like inflation in the early universe but evolve in much smaller energy scales and can give rise to late time acceleration irrespecetive of the form of potential but with certain initial conditions.

We set up a very general autonomous system of equations involving both the background as well as the perturbed universe. This is valid for any form of the potential irrespective of whether it is thawer model or tracker model. Subsequently we solve the autonomous system of

equations with thawing type initial conditions for the scalar field evolution. Our main aim is to see effect of thawing scalar fields on observed galaxy power spectrum on large scales with different GR corrections and compare it to the ΛCDM model.

We study the deviation in different physical quantities related to perturbed universe from ΛCDM model. Finally we study the contribution of each of these quantities in the observed galaxy power spectrum taking into account different GR corrections. Our study shows that on very large scales ($k = 0.0001 Mpc^{-1}$), there can be upto $15 - 20\%$ deviation from the ΛCDM in the observed galaxy power spectra depending upon the choice of the potential. Inverse-squared potential is the most promising one to be distinguished from ΛCDM as it has the highest deviation. Even if one considers the limitation to probe such large scales due to cosmic variance, $15 - 20\%$ deviations from ΛCDM model are always encouraging. Within individual potential, we have a $2 - 5\%$ deviations which is not as big as that from ΛCDM. Also this deviation from ΛCDM is non-monotonic. For larger scales, we have an enhancement of power from ΛCDM and then as we go to smaller scales, we get a suppression of power from ΛCDM for smaller redshifts which again changes to enhancement of power for larger redshifts. The change over redshift is quite robust in terms of different potentials and for different choice of cosmological parameters and always happens around $z \sim 1.2$. We believe this change of slope in galaxy power spectrum with respect of ΛCDM model is a distinguishable feature for thawing class of models (as of now, we are not aware of any such previous results) and needs to be probed further. In near future, we plan to study this effect for more diverse class of scalar field models.

6 ACKNOWLEDGEMENTS

B.R.D. thanks CSIR, Govt. of India for financial support through SRF scheme (No:09/466(0157)/2012-EMR-I). A.A.S acknowledges the support provided by Abdus Salam International Center For Theoretical Physics, Trieste, Italy through its Associate Program, where part of the work has been done. The authors also thank Sumit Kumar for valuable inputs regarding the python programming for the computational part of the problem. We also acknowledge the usage of HOPE-A Python Just-In-Time compiler for astrophysical computations (Akeret et al. 2015) for our computation.

REFERENCES

Abell P. A., et al., 2009, preprint (arXiv:0912.0201)
Ade P. A. R., et al., 2015a, preprint (arXiv:1502.01589)
Ade P. A. R., et al., 2015b, preprint (arXiv:1502.01590)
Akeret J., Gamper L., Amara A., Refregier A., 2015, Astronomy and Computing, 10, 1
Alam S., et al., 2016, preprint (arXiv:1607.03155)
Ali A., Sami M., Sen A. A., 2009, Phys. Rev., D79, 123501
Bagdonaite J., Ubachs W., Murphy M. T., Whitmore J. B., 2015, Phys. Rev. Lett., 114, 071301
Bertacca D., Maartens R., Raccanelli A., Clarkson C., 2012, JCAP, 1210, 025
Betoule M., et al., 2014, Astron. Astrophys., 568, A22
Bonvin C., 2014, Class. Quant. Grav., 31, 234002
Bonvin C., Durrer R., 2011, Phys. Rev., D84, 063505
Bonvin V., et al., 2016, preprint (arXiv:1607.01790)
Caldwell R. R., Linder E. V., 2005, Phys. Rev. Lett., 95, 141301
Caldwell R. R., Dave R., Steinhardt P. J., 1998, Physical Review Letters, 80, 1582
Challinor A., Lewis A., 2011, Phys. Rev., D84, 043516
Copeland E. J., Sami M., Tsujikawa S., 2006, International Journal of Modern Physics D, 15, 1753
Delubac T., et al., 2015, A&A, 574, A59
Duniya D., 2016, preprint (arXiv:1606.00712)
Duniya D., Bertacca D., Maartens R., 2013, JCAP, 1310, 015
Duniya D. G. A., Bertacca D., Maartens R., 2015, Phys. Rev., D91, 063530
Hossain M. W., Sen A. A., 2012, Phys. Lett., B713, 140
Jeong D., Schmidt F., Hirata C. M., 2012, Phys. Rev., D85, 023504
Kaiser N., 1987, Mon. Not. Roy. Astron. Soc., 227, 1
Li D., Scherrer R. J., 2016, Phys. Rev., D93, 083509
Liddle A. R., Scherrer R. J., 1999, Phys. Rev. D , 59, 023509
Linder E. V., 2015, Phys. Rev., D91, 063006
Maartens R., Abdalla F. B., Jarvis M., Santos M. G., 2015, PoS, AASKA14, 016
Moessner R., Jain B., Villumsen J. V., 1998, Mon. Not. Roy. Astron. Soc., 294, 291
Padmanabhan T., 2003, Phys. Rep., 380, 235
Peebles P. J., Ratra B., 2003, Reviews of Modern Physics, 75, 559
Perlmutter S., et al., 1997, Astrophys. J., 483, 565
Ratra B., Peebles P. J. E., 1988, Phys. Rev. D , 37, 3406
Riess A. G., et al., 1998, Astron. J., 116, 1009
Riess A. G., et al., 2016, preprint (arXiv:1604.01424)
Sahni V., Starobinsky A., 2000, International Journal of Modern Physics D, 9, 373
Sahni V., Shafieloo A., Starobinsky A. A., 2014, ApJ, 793, L40
Scherrer R. J., Sen A. A., 2008, Phys. Rev., D77, 083515

Steinhardt P. J., Wang L., Zlatev I., 1999, Phys. Rev. D , 59, 123504
Tsujikawa S., 2010, Lect. Notes Phys., 800, 99
Unnikrishnan S., Jassal H. K., Seshadri T. R., 2008, Phys. Rev. D , 78, 123504
Wetterich C., 1988, Nucl. Phys., B302, 668
Yoo J., Fitzpatrick A. L., Zaldarriaga M., 2009, Phys. Rev., D80, 083514
Yoo J., Hamaus N., Seljak U., Zaldarriaga M., 2012, Phys. Rev., D86, 063514